NURETH-21 21st International Topical Meeting on Nuclear Reactor Thermal Hydraulics
August 31 (Sun) - September 5 (Fri), 2025
BEXCO · Busan, Korea
www.nureth-21.org

Novel Heat Transfer Models to improve the Performance Prediction of Passive Residual Heat Transfer Systems

Tahmineh Adili, Yu Zhang, Iurii Dolganov and Stephan Leyer
University of Luxembourg
Campus Kirchberg, 6, rue R. Coudenhove-Kalergi, 1359 Luxembourg, LuxemburgA@institute.gov;
stephan.leyer@uni.lu

ABSTRACT

Passive safety systems are an economically interesting alternative to conventional active systems, which are also more robust against many external influences, as they do not rely on an external, active drive. Accordingly, they continue to function even if large parts of the plant infrastructure are damaged or unavailable, as it was the case in Fukushima Daiichi accident, for example. However, passive heat removal systems in particular pose major challenges for designers and the thermal-hydraulic calculation tools they use. One reason for this is the coupling or feedback between the heat flow that is introduced into the coolant and the mass flow of the coolant through the system, which results from the heat input. In addition, state-of-the-art heat transfer models obviously cannot capture the heat transfer for passive systems precisely enough. As a result, attempts to recalculate experimentally determined heat transfer rates of passive heat removal systems with fluid dynamic codes have sometimes resulted in considerable deviations between experimental and numerical data. This paper presents two new heat transfer models developed specifically for passive systems. It describes how they can help to better calculate and predict the performance of related systems. The models were developed primarily based on experimental data recorded at the COSMEA and NOKO test stands and published by the Helmholz Center Dresden Rossendorf. In addition, the model development was supported by CFD calculations executed to better understand the underlying mechanisms.

KEYWORDS
Nuclear Safety, Passive Residual Heat Removal Systems, Heat Transfer Models, Multi-Phase Flow, Condensation

1. INTRODUCTION

Despite the affordable, low-carbon electricity provision offered by the operation of nuclear power plants, their acceptance strongly depends on their safe operation. This is linked to the enormous risk potential and the environmental impact related to the release of radioactive material to the environment. In the cause of the operation of nuclear power plants (NPP) starting with the first Generation I reactors in the early 60th of the 20th century to the modern Generation III and III+ reactors recently being built several accidents have happened, some of which were related to larger releases of radioactive material. The accident of unit 3 of the Three Mile Island NPP in 1979 for example represented a major milestone in reconsidering nuclear reactor safety concepts. As a consequence, substantial safety uprates have been developed and introduced in many countries operating NPPs. Examples are the inclusion of severe accident mitigation measures, hardened safety

requirements against external hazards, or diversified safety systems. Passive safety equipment represents an interesting supplement or alternative to active safety systems [1, 2, 3]. They operate without external energy supply and their simplicity in design contributes to a reduction of investment costs. Moreover, the operational independence from the external power supply reduces the likelihood of system failures. Probabilistically the combination of active and passive systems relying on significantly different operating principles reduces the core damage frequency significantly [4]. However, many of the passive safety systems currently being applied in Generation III and III+ reactors suffer from a lack of operational experience. In contrast to service-proven active designs, relatively few experiences with passive systems are available. The information is mostly limited to isolated passive systems applied already in previous reactor designs and the experimental and numerical system analysis [2, 5]. A passive system taking over most or even all safety functions in a nuclear power plant is a characteristic of many new Generation III and III+ designs. Consequently, the assessment of a passive safety concept relies on the numerical assessment of accident scenarios performed with state-of-the-art thermohydraulic codes. Related to the comparatively low driving forces, the related tendency to unstable operation [6, 7], the huge operation parameter field, and the fact that many models implemented in fluid dynamics codes are specifically developed for active systems, passive safety systems challenge the state of the art design tools like thermohydraulic system codes. This applies in particular to passive residual heat removal systems (PRHR). Such systems rely typically on natural circulation flows for which the heat transfer into and out of the system triggers the fluid density and hence provides the system mass flow. Consequently, accurate determination of the heat transfer is crucial for the proper assessment of such systems.

Two distinct PRHR are typically found in LWRs. The low-pressure systems are used to discharge heat introduced into the containment of a reactor to the heat sink used for passive accident management. High pressure passive residual heat removal systems (HPRHR) are devoted to discharging heat from the reactor pressure vessel (RPV) (in case of BWR) or the Primary System (in case of PWR) to either the containment or even directly to the ultimate heat sink [1]. Several different designs have been developed, some of which are equipped with heat exchangers with horizontal, inclined, or vertical condenser tubes. The KERENA Emergency Condenser (EC) has been selected as the reference design for this study. It represents an example of a U-tube heat exchanger with slightly inclined tubes. The Condenser consists of 61 tubes submerged in the Core Flooding Pools of the Containment. Recently performed numerical assessments of such systems using fluid dynamic system codes showed a significant discrepancy between the numerically and experimentally predicted heat transfer capacities [5, 8, 9]. Within the present study the development of an improved heat transfer model for the primary- and secondary-side heat transfer determination for horizontal or slightly inclined heat exchanger tubes for HPRHR systems is presented. This development is based on the further development of state-of-the-art models, experimental data as well as Computational Fluid Dynamic (CFD) data.

The paper is organized into four sections. After the introduction, chapters 2 and 3 introduce the state-of-the-art heat transfer models and the development of new modified models for the heat transfer inside and outside the heat exchanger tubes. It also includes a brief introduction of the experimental setups and data used as the basis for model development. The final part provides a summary and an outlook on future activities.

2. PRIMARY SIDE HEAT TRANSFER MODEL DEVELOPMENT

The heat transfer via the EC Tubes is determined by the driving temperature difference between inside and outside the heat exchanger tube, but also by the thermal resistance consisting of the convective

heat transfer on the inside and outside the heat exchanger tubes. In addition, comes heat conduction via the tube wall. Inside the tubes, the convective heat transfer is a superposition of steam condensation and single-phase liquid convective heat transfer. On the outside, it is a superposition of again single-phase liquid convection and evaporation. This chapter focuses on the modelling of the inner side, in the following called primary side (PS). Chapter 3 will deal with the secondary side (SS) outside the tube. This chapter will start with an introduction to state-of-the-art heat transfer models and show their performance in capturing heat transfer capacity. On this basis, an optimized new heat transfer model for the PS will be derived.

2.1. Primary Side Heat Transfer Modelling

Since the heat transfer represents a superposition of steam condensation and single-phase convection, the distribution of the phases and the rustling contact of steam to cooled structures or the liquid phase strongly impact the heat transfer rates. Successful heat transfer models need to correctly account for the phase distribution. Figure 1 shows the development of the phase distribution in a horizontal tube that is exposed to a steam flow at the entrance and that is cooled via the wall so that the void fraction decreases in the axial direction [10]. The heat transfer results in the formation of droplets that accumulate on the tube walls forming a liquid ring that can be sustained as long as the flow velocities are high enough. The corresponding flow structure is called annular flow. As a consequence of the decreasing void fraction, the flow is decelerated so that the symmetric annulus can no longer be sustained a drainage flow accumulates in the lower part of the tube. The subcooling of the drainage provides an important contribution to the driving force of the natural circulation system. Further downstream the void fraction has reached values sufficiently small to create slugs and bubbles. After all steam factions have been condensed the flow is purely a single-phased liquid that is subcooled by the continuing heat transfer.

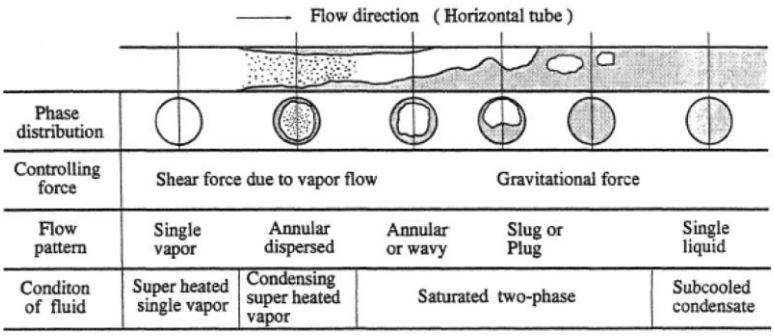

Figure 1. Flow morphology during condensation in a horizontal tube [10].

Several suitable heat transfer models have been proposed in previous works for condensation in horizontal or slightly inclined heat exchanger tubes. A summary can be found in [11, 12]. In this chapter, the suitable models for the heat transfer analysis of the COSMEA experiments are summarized. These experimental data serve as databases for the assessment of the state-of-the-art PS models and the development of the new model in this paper. A brief description of the facility is given in subsection 2.1.3. A more detailed description can be found in [13]. The models can be divided into two groups. Group I models neglect the contribution of the drainage flow in the lower part of the heat exchanger tube while the group II model considers this contribution.

2.1.1. Summary of Group I Type Models

Chato [14] developed a model based on the Nusselt Theory [15] and experimental data using refrigerants for horizontal and inclined heat exchanger tubes (equation 1). The model is valid for Reynolds numbers: $Re \leq 35000$.

$$\mathrm{h} = \mathrm{F}(\theta) \cdot \left[\frac{\rho_l \cdot (\rho_l - \rho_v) \cdot g \cdot h_{lv} \cdot \lambda_l^3}{\mu_l \cdot D \cdot (T_s - T_w)}\right]^{1/4} = 0.296 \cdot \left[\frac{\rho_l \cdot (\rho_l - \rho_v) \cdot g \cdot \Delta i_{lv} \cdot \lambda_l^3}{\mu_l \cdot D \cdot (T_s - T_w)}\right]^{1/4} \quad (1)$$

For the application in the ATHELT Code [16] the Chato model was modified in a way that the constant factor F was replaced by a pre-factor that considers the level of the void fraction and the corresponding level of the drainage flow [17].

Modified Chato Model:

$$\mathrm{h} = 0.728 \cdot \varepsilon_{mod.} \cdot \left[\frac{\rho_l \cdot (\rho_l - \rho_v) \cdot g \cdot \Delta i_{lv} \cdot \lambda_l^3}{\mu_l \cdot D \cdot (T_s - T_w)}\right]^{1/4} \quad (2)$$

Validation range is given as: $0 < x_H$ and $0.995 \geq \varepsilon$.

An approach similar to the one used for the Modified Chato Model was chosen by Kosky and Staub [18]:

$$\mathrm{h} = 0.725 \cdot \left[\frac{\rho_l \cdot (\rho_l - \rho_v) \cdot g \cdot \Delta i_{lv} \cdot \lambda_l^3}{\mu_l \cdot D \cdot (T_s - T_w)} \cdot \varepsilon_{mod.}^3\right]^{1/4}, \quad \varepsilon_{mod.} = \left[1 + \left((1-x)/x\right) \cdot (\rho_v/\rho_l)^{2/3}\right]^{-1} \quad (3)$$

The parameter range for its application is limited to: $1.2\ MPa \leq P \leq 20 MPa$, $400\ kg/\dot{m}^2 s \leq \dot{G}_l \leq 2000\ kg/m^2 s$, $13\ \mathrm{mm} \leq D \leq 20\ mm$.

One further similar model was proposed by Szijarto et.al. [19]. The validation is based on the INVEP experimental data. The pre-factor was explicitly expressed as function of the stratification angle:

$$\mathrm{h} = \mathrm{F} \cdot \left[\frac{\rho_l \cdot (\rho_l - \rho_v) \cdot g \cdot \Delta i_{lv} \cdot \lambda_l^3}{\mu_l \cdot D \cdot (T_s - T_w)}\right]^{1/4}, \quad \mathrm{F} = -0.102 + 0.9017\theta \quad - 0.0257\theta^3 \quad (4)$$

Corresponding to the Chato model the application range of this model is limited to Reynolds Numbers below 35000.

2.1.2. Summary of Group II Type Models

The characteristic of the 2nd group of condensation models is that the convective heat transfer caused by the drainage flow is considered.

Dobson and Chato [20] performed condensation experiments and derived a heat transfer model for both annular and stratified wavy flow regimes.

$$\mathrm{h} = \left[\frac{0.023 Re_{vo}^{0.12}}{1 + 1.1 X_{tt}^{0.58}} \left[\frac{GaPr_l}{Ja_l}\right]^{0.25} + \left(1 - \frac{\theta}{\pi}\right) \left[0.0195 Re_l^{0.8} Pr_l^{0.4} \sqrt{1.376 + \frac{C_1}{X_{tt}^{C_2}}}\right]\right] \cdot \left(\frac{\lambda_l}{D}\right)$$

$$1 - \frac{\theta}{\pi} = \frac{\arccos\left(2\varepsilon_{mod.} - 1\right)}{\pi}, \quad Fr_l > 0.7 : C_1 = 7.242, C_2 = 1.655 \quad (5)$$

$$Fr_l \leq 0.7 : C_1 4.172 + 5.48 Fr_l - 1.564 Fr_l^2, \; C_2 = 1.733 - 0.169 Fr_l$$

The model contains two terms accounting for the film condensation in the upper part of the tube and for single-phased convection heat transfer in the lower part. The application parameter range for the Dobson and Chato Model is specified as follows:

$$75\ kg/\dot{m}^2 s \leq \dot{G}_l \leq 500\ kg/m^2 s; \qquad 3.14\ \mathrm{mm} \leq D \leq 20\ mm$$

Cavalini provided two different models based on experimental data using refrigerants [21, 22]. The first model considers also condensation in the upper and convection heat transfer in the lower part of the tube:

$$\mathrm{h} = 0.725\left[\frac{\rho_l\cdot(\rho_l-\rho_v)\cdot g\cdot\Delta i_{lv}\cdot\lambda_l^3}{\mu_l\cdot D\cdot(T_s-T_w)}\right]^{1/4}\left[1+0.82\left(\frac{1-x}{x}\right)^{0.268}\right]^{-1}+h_{LO}(1-x)^{0.8}\left(1-\frac{\theta_{strat}}{\pi}\right) \quad (6)$$

$$h_{LO} = 0.023Re_l^{0.8}Pr_l^{0.4}\left(\frac{k_l}{D}\right)$$

The parameter application range is limited to:

$30\ ℃ \le T_s \le 50\ ℃;\qquad 100\ kg/\dot{m}^2s \le \dot{G}_l \le 750\ kg/m^2s$

The second model proposed by Cavalini distinguishes between heat transfer in which the temperature difference is the dominating parameter for the heat transfer resistance and flow regimes in which the heat transfer rate is largely independent on the temperature difference:

$$\mathrm{h}=\left[h_A\left(\frac{J_v^T}{J_v}\right)^{0.8}-h_{strat}\right]\left(\frac{J_v^T}{J_v}\right)+h_{strat}$$

$$h_A = h_{LO}\left[1+1.128x^{0.817}\left(\frac{\rho_l}{\rho_v}\right)^{0.3685}\left(\frac{\mu_l}{\mu_v}\right)^{0.2363}\left(1-\frac{\mu_l}{\mu_v}\right)^{2.144}Pr_l^{-0.1}\right] \quad (7)$$

$$h_{strat} = 0.725\left[1+0.741\left(\frac{1-\varepsilon}{\varepsilon}\right)^{0.3321}\right]^{-1}\left[\frac{\rho_l\cdot(\rho_l-\rho_v)\cdot g\cdot\Delta i_{lv}\cdot\lambda_l^3}{\mu_l\cdot D\cdot(T_s-T_w)}\right]^{1/4}+(1-\varepsilon^{0.087})h_{LO}$$

Another model distinguishing between condensation and convection is provided by Shah [23]:

$$\mathrm{Z}=\left(\frac{1}{\mathrm{x}}-1\right)^{0.8}P_r^{0.4};\qquad h_{LS}=0.023\frac{\lambda_l}{D_h}Re_l^{0.8}Pr_l^{0.4}$$

$$h_1 = h_{LS}\left(\frac{\mu_l}{14\mu_v}\right)^{0.0058+0.557P_r}\cdot\left[(1-\varepsilon)^{0.8}+\frac{3.8\varepsilon^{0.76}(1-x)^{0.04}}{P_r^{0.38}}\right] \quad (8)$$

$$h_2 = 1.32Re_l^{-1/3}\left[\frac{g\rho_l(\rho_l-\rho_v)\lambda_l^3}{\mu_l^2}\right]^{1/3}$$

In regime I: $J_v \le \frac{1}{2.4Z+0.73}$ $\qquad h = h_1$

In regime II: $0.89-0.93\exp(-0.087Z^{-1.17}) \ge J_v \ge \frac{1}{2.4Z+0.73}$ $\qquad h = h_1 + h_2$

For horizontal tubes, the equation is recommended only if $Re_{TP} > 35000$

In regime III: $J_v \le 0.89-0.93\exp(-0.087Z^{-1.17})$ $\qquad h = h_2$

The model can be applied under the following conditions:

$0.0008 \le P_r \le 0.9;\qquad 4\ kg/\dot{m}^2s \le \dot{G}_l \le 820\ kg/m^2s;\quad 2\ \mathrm{mm} \le D \le 49\ mm$

$68 \le Re \le 85000;\qquad 1 \le Pr \le 18$

Ahn et al. [24] proposed an improved condensation model based on the regression analysis of experimental data of steam condensation (equation 9). The model consists of an interface shape prediction mode and a condensation heat transfer coefficient model.

$$h_f = 0.729\left(1+8.7\cdot10^{-4}Re_l^{0.57}\right)\left[\frac{\rho_l\cdot(\rho_l-\rho_v)\cdot g\cdot\Delta i_{lv}\cdot\lambda_l^3}{\mu_l\cdot D\cdot(T_s-T_w)}\right]^{\frac{1}{4}}$$

$$h = \frac{h_f(2\pi-\theta)+h_{LO}\theta}{2\pi} \quad (9)$$

The model is valid for the following parameter ranges:

$27.5\ \mathrm{mm} \le D \le 44.8\ mm;\ 10\ kg/\dot{m}^2s \le \dot{G}_l \le 329\ kg/m^2s<;\ 0.02 \le P_r \le 0.3$

2.1.3. Assessment of state-of-the-art heat transfer models using ATHELT

In order to assess the performance of the models presented in subsections 2.1.1 and 2.1.2 ATHLET calculations have been performed and compared with the experimental data recorder at the COSEMA

test facility at the Helmholtz Zentrum Dresden Rossendorf (HZDR). ATHLET [16] is a thermal-hydraulic system code, which is being developed by the "Gesellschaft für Anlagen- und Reaktorsicherheit" (GRS). The spatial discretization scheme of ATHLET is based on the 1-D finite-volume staggered grid approach. ATHELT provides a Python interface that was used to include the heat transfer condensation models described before. A detailed description of the calculation model used is presented in [25]. The experimental data used for the assessment of the heat transfer models are recorded at the COSMEA (COndenSation test rig for flow Morphology and hEAt transfer studies) test facility. The following description of the facility will focus on the features essential for the present work. [13] provides a more detailed description of the facility. The system consists of a mixing zone that allows preconditioning the 2-phase flow with tunable entrance void fraction. Subsequently, the flow can fully develop in an adiabatic pipe section before it enters the condenser tube. The secondary side of the condenser tube is cooled by a forced convection-swirled liquid water flow. The swirl elements guarantee a uniform temperature profile along the circumference. In addition to the temperature, pressure, and mass flow sensors the facility is equipped with an x-ray tomograph to measure fife different locations and distribution of liquid and vapor phase. At one position the flow morphology information is supplemented by heat transfer measurements with an angular resolution of 22.5 °. The combination of the phase distribution and the angular dependence of heat flux provides a unique database for the assessment of related heat transfer models and the development of new models. The standard ATHELT setup uses the modified Chato Model (equation 2). To assess in addition the performance of the further heat transfer models described in the previous subsection the code provides the possibility to implement additional heat transfer models via a Python interface. This interface allows the exchange of thermohydraulic data and the related calculation of the heat transfer coefficient. In Figure 2 the measured and calculated heat flux versus the pipe inlet steam mass fraction is plotted for varying primary side system pressures. The calculations have been performed by fixing the outer condenser tube wall temperature to the value extracted from the measurements. This procedure eliminated influences coming from uncertainties related to the secondary side heat transfer coefficient. The data reveal a systematic underestimation of the calculated heat flux with respect to the measured one. The averaged deviations are listed in Table I. Obviously, the models belonging to group II considering the contribution of the convective heat transfer by the drainage flow in the lower part of the tube perform better than the group I models. The deviation between the calculated and measured heat flux only weakly depends on the void fraction for group I models. However, all models belonging to group II show a significant drop of the calculated heat flux for small void fractions, except the Cavallini Model from 2006. A likely explanation is that the contribution of the convective heat transfer plays an important role so that group I models fail. Nevertheless, the contribution needs to be considered correctly. Hence also group II models fail if it does not reflect the flow conditions, phase distribution, and the resulting heat transport phenomena properly.

Table I. Deviations of Simulation results

Model	Chato (1962)	Jaster and Kosky (1976)	Modified Chato	Szijarto (2015)	Dobson and Chato (1998)
Deviation[%]	42.05%	36.66%	36.66%	34.12%	24.41%
Model	Cavallini (2002)	Cavallini (2006)	Ahn (2014)	Shah (2008)	
Deviation[%]	40.01%	16.81%	30.63%	31.91%	

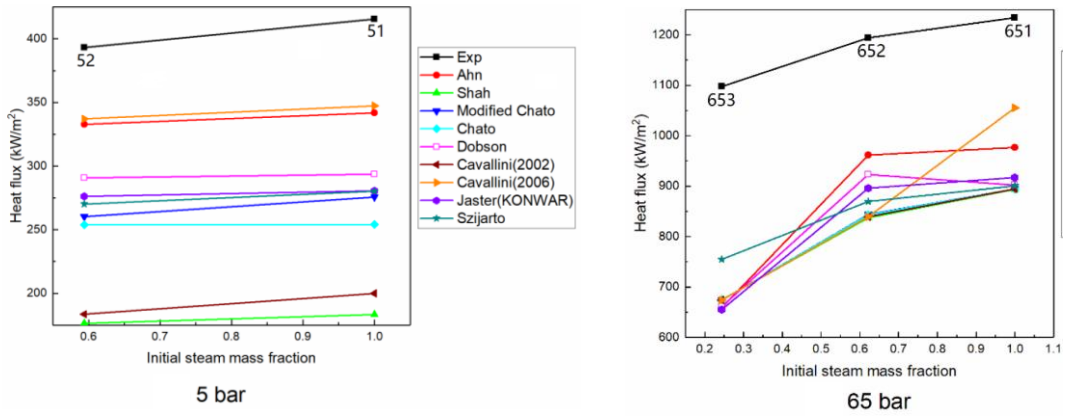

Figure 2. Comparison of measured (COSMEA) and calculated local heat flux (further pressure data can be found in [25]).

As a consequence of the observation, a new model based on COSEMA, as well as further data available in the literature, have been derived. The model and its validation will be described in section 2.2.

2.2. Heat Transfer Model Development

In [25] a sensitivity analysis of the main input parameters has been executed that unrevealed that the void fraction and the mass flow are the dominating parameters. These parameters determine the flow structure, the distribution, and the interaction of the phases as well as their thermal contact to the heat transfer structures. This is why the newly developed model is chosen to consider the flow structure distinguishing between the annular flow regime, stratified regime (considering the interfacial shear force - so-called 'wavy effect'), and the transition regime between the annular and stratified flow regime. The criteria for the three different regimes are taken from the Tandon flow map [26]:

- Annular flow $1.7 < j_g < 6$ and $(1-\varepsilon)/\varepsilon \leq 0.5$
- Transition flow $0.7 \leq j_g \leq 1.7$ and $(1-\varepsilon)/\varepsilon \leq 0.5$
- Stratified flow $0 \leq j_g \leq 0.7$ and $(1-\varepsilon)/\varepsilon \leq 0.5$

Here j_g is the dimensionless gas velocity: $j_g = \frac{x\dot{m}}{\sqrt{gD(\rho_l-\rho_g)\rho_g}}$. Furthermore, the hydraulic diameter used in the model is redefined considering the real phase occupation of the pipe cross-section. In the following, the different sub-models and the validation of the model are described.

2.2.1. Sub-Model for the annular flow regime

The thermal contact of vapor with the colder tube wall causes wall condensation forming a film along the wall. If the vapor velocity is high enough to carry the liquid film, the annulus film is sustained. For such conditions, Nusselt has proposed a related condensation model [15]. To consider the effect of a wavy interface between the liquid annulus and the vapor core the model is uprated introducing a prefactor considering the Reynold number of the vapor flow Re_g:

$$h_{ann.} = 0.729 \cdot f(Re_g) \left[\frac{\rho_l \cdot (\rho_l - \rho_v) \cdot g \cdot \Delta i_{lv} \cdot \lambda_l^3}{\mu_l \cdot D \cdot (T_s - T_w)}\right]^{\frac{1}{4}} \quad (10)$$

Where:

$$Re_g = \frac{GxD_{hg}}{\mu_g \varepsilon} \tag{11}$$

$D_{hg} = \frac{4A_g}{S_g}$ is the thermal-hydraulic diameter of the vapor dominating the interfacial shear force and S_g wetting perimeter length of steam. The determination of the function $f(\mathrm{Re_g})$ has been done using the machine learning regression analysis method via MATLAB. The regression equation (10) is rearranged as follows:

$$f(Re_g) = \frac{h_{ann.}}{0.729 \cdot \left[\frac{\rho_l \cdot (\rho_l - \rho_v) \cdot g \cdot \Delta i_{lv} \cdot \lambda_l^3}{\mu_l \cdot D \cdot (T_s - T_w)}\right]^{\frac{1}{4}}} = \frac{h_{ann.}}{b} \tag{12}$$

For the regression, the COSEMA data were supplemented by further suitable experimental data published in literature [27, 28, 29]. The regression procedure provided the following formula [25]:

$$f(Re_g) = 1.26 + 1.163 \cdot 10^{-6} Re_g^{1.183} \tag{13}$$

2.2.2. Sub-Model for the stratified flow regime

The stratified flow regime model consists of two parts as indicated in Figure 3: condensation heat transfer applying equation (10) for the upper part of the tube and convective heat transfer in the lower part of the tube. However, to combine both heat transfer phenomena, the hydraulic diameter and the pipe cross-section occupied by steam A_g needs to be defined. This is done by introducing the stratification angle (see Figure 3).

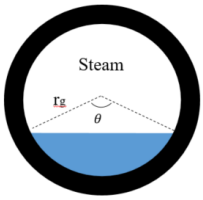

Figure 3. Sketch of the stratified flow regime phase distribution

From the definition of the angel θ one can calculate A_g and s_g:

$$A_g = \pi r_g^2 - \frac{\theta}{2} r_g^2 + \sin\frac{\theta}{2} \cdot \cos\frac{\theta}{2} \cdot r_g^2 \tag{14}$$

$$s_g = r_g(2\pi - \theta) + 2\, r_g \sin\frac{\theta}{2} \tag{15}$$

The stratified angle was computed using the following correlation proposed by Hart et al. [30]:

$$\theta = 2\pi[0.52(1-\varepsilon)^{0.374} + 0.26Fr^{0.58}] \tag{16}$$

The Froude number Fr in Equation (16) is defined as follow:

$$Fr = \frac{\rho_l u_l^2}{(\rho_l - \rho_g) g D_h} \tag{17}$$

The Dittus and Boelter [31] heat transfer correlation (equation 18) was chosen as a basis for the convective heat transfer coefficient determination for the drainage flow in the lower part of the heat exchanger tube under stratified flow conditions.

$$h_{conv.} = C \cdot \frac{\lambda}{D_{hl}} \cdot Re_l^{0.8} \cdot Pr_l^{0.4} \tag{18}$$

However, the constant C in equation (18) was determined by a regression analysis method applied to the COSMEA experimental data. As a result, the value for the constant was set to: $C = 0.4511$ [25]. The circumference averaged stratified flow heat transfer coefficient is calculated by adding the stratified angle weighted average of the heat transfer coefficients of film condensation and heat convection:

$$h_{strat} = \frac{h_{ann.}(2\pi - \theta) + h_{conv} \cdot \theta}{2\pi} \tag{19}$$

2.2.3. Sub-Model for the transition regime between annular and stratified flow

In the transition regime, a linear interpolation between the models for annular flow (equation 10) and stratified flow (equation 19) was chosen. The application range for the sub-models was again taken for the Tandon flow map [26]. The boundary values were taken as:

$$h_{ann.} = h_{ann.}(j_g = 1.7) \quad \text{and} \quad h_{strat} = h_{strat}(j_g = 0.7) \tag{20}$$

This the heat transfer coefficient for the transition regime is calculated by:

$$h_{tran.} = f \cdot (h_{ann.} - h_{strat}) + h_{strat} \qquad \text{with} \quad f = \frac{J_g - 0.7}{1.7 - 0.7} \tag{21}$$

2.2.4. Validation of the new model

The post-calculation of the COSMEA experiments has been repeated using the same ATHLET setup but by implementing the new model into the calculation via the ATHELT Python interface. The comparisons between the measured and the calculated heat flux using the new model are plotted in

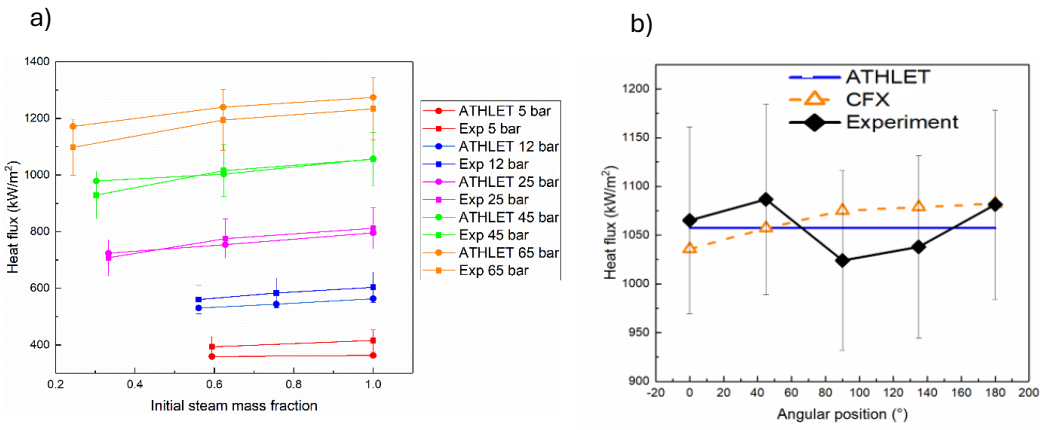

Figure 4: a) Comparison of the local heat flux measurement (COSMEA) and calculation applying the new model. b) Heat Flux as function of the angular direction. Comparison of the COSEMA experimental, CFD and ATHLET calculation results.

Figure 4 as a function of the initial void fraction for different primary side pressure levels. The averaged error is now decreased to values below 5 % so that the deviation has dropped to values smaller than the experimental uncertainties. The improvement can be understood by comparing the angular resolved heat flux shown in Figure 4 b. There the experimental data taken from the COSMEA (experiment number 451, 45 bar) heat flux probe measurements, the CFX calculation data taken for [32], and the ATHELT heat flux calculation using the new model are compared. The experimental as well as the CFD data show only a weak dependence on the angular direction. The mean value of both

the CFD and the experimental data is captured quite well by the ATHELT calculation results. A more detailed validation of the model is given in [25]. In summary, the new model application leads to a significant improvement of the heat flux prediction by ATHLET for passive safety systems using horizontal or slightly inclined heat exchanger tubes.

3. SECONDARY SIDE HEAT TRANSFER MODEL DEVELOPMENT

For the secondary side, representing a tube bundle submerged in a pool several heat transfer models are proposed in the literature. In [33] a survey of such models is resented. Among those models, the ones listed in table II are selected to be the most suitable to capture the specifics of the secondary side of the EC. The selection of these models is based on their application range and their development specifically for nucleate pool boiling in large volumes of coolant.

Table II. Selected state of the art heat transfer models for the EC SS heat transfer calculation.

Model	Formula	Application Range
Kutateladze [34]	$Nu = 0.44K_*^{0.7}Pr^{0.35}$ $h = 0.44 \cdot \left(\frac{\lambda}{l_*}\right) \cdot \left[\frac{10^{-4}q_F p_{sat}}{gr\rho_{st}\mu} \cdot \frac{\rho_w}{\rho_w - \rho_{st}}\right]^{0.7} \cdot Pr^{0.35}$	Large volume water, clean flat heating surfaces, pressure between 1 to 225 bar.
Rohsenow [35]	$\frac{c_p \Delta T_b}{r} = C_{sf}\left[\frac{q_F l_*}{\mu r}\right]^{0.33}\left(\frac{c_p \mu}{\lambda}\right)^n;\ h = \frac{q_F}{\Delta T_b}$ $C_{sf} = 0.008, \quad n = 1$	Large volume water and other coolants (such as Ethanol, R-113, and n-Heptane), a plate heating surface, Pressure between 1 to170 bar
Kruzhilin [36]	$h = 0.082\left[\frac{q_F r}{gT_{sat}\lambda} \cdot \frac{\rho_{st}}{\rho_w - \rho_{st}}\right]^{0.7}\left[\frac{T_{sat}c_p\sigma\rho_w}{r^2{\rho_{st}}^2 l_*}\right]^{0.33}\left(\frac{\lambda}{l_*}\right)Pr^{-0.45}$	Large volume water and other coolants, a thick metal plate heating surface with different materials (Copper, Aluminum, Brass, Chromium and St.St.),
Labuntsov [37]	$h = 0.075\left[1 + 10\left(\frac{\rho_{st}}{\rho_w - \rho_{st}}\right)^{0.67}\right]\left(\frac{\lambda^2}{\sigma \upsilon T_{sat}}\right)^{0.33} {q_F}^{0.67}$ Or $Nu = 2{,}63^{-2}\left(\frac{\lambda \Delta T}{r\rho_{st}\upsilon}\right)^{1.86} \cdot Pr^{0.952}$	Large volume water and other coolants, a thick metal plate heating surface with different surface material and roughness.

For the assessment of these models the experimental data recorded at the Noko test facility at the HZDR were used to test the performance of these models.

3.1. The Noko-Test facility

The Noko test facility was initially set up and operated at the Jülich Research Center in Germany. It was later transferred to the HZDR and connected to the TOPFLOW system there. The test rig is a mockup of the KERNEA EC with a heat exchanger tube bundle consisting of eight, ten meter long, U-shaped heat exchanger tubes installed in a water tank that serves as a heat sink. The maximum heating power is 4 MW and the maximum pressure on the primary side is 7 MPa. The instrumentation allows to measure the temperature field inside the water tank with a high spatial resolution and is therefore appropriate for the validation of CFD data. The test data listed in table III were used for the assessment of the state-of-the-art heat transfer models as well as for the determination of an improved model.

Table III. Noko test matrix (P_{Prim}: Primary Side Pressure; T_{Sec}: Secondary Side Temperature)

Experiment	P_{Prim} [MPa]	T_{Sec} [°C]	P [MW]
1	1.0	32.5	1.35
2	3.0	20.0	2.454
3	5.0	22.0	3.177
4	6.5	25.5	4.011

The tests were executed by defining the primary side system pressure and the secondary side water temperature. The tests were started by opening the valve in the EC outflow line. Steam enters the heat exchanger, and heat is transferred to the water in the vessel. To keep the secondary side pressure constant heat was introduced into the pressure vessel feeding the EC. Depending on the test parameter it took between 1000 and 2100 seconds until steady state conditions on the PS of the EC were reached. A detailed description of the test facility and the experiments executed at the facility can be found in [38, 39]. Based on the experimental data CFD calculations have been performed to determine the temperature profile and the heat transfer. The description of these calculations is beyond the scope of this paper. The details can be found in [33]. However, the data have been used as input and for comparison to assess the quality of the new model derived for the SS heat transfer coefficient. To determine the heat transfer coefficient via the models listed in Table II and from the experimental data it was necessary to derive the outer wall temperature, the bulk water temperature in the vessel and for the experimental data also the heat flux transferred via the EC. For the later one the heating Power introduced into the presser vessel of the Noko Test facility under steady-state conditions was divided by the heat transfer in the surface of the heat exchanger tubes. The mean value of the bulk water temperature in the vessel was either determined via the temperature measurements in the vessel or from the temperature field CFD calculation [33]. The mean value of the outer wall temperature of the heat exchanger was determined from the fluid temperature inside the heat exchanger tubes and the heat transfer via the pipe wall. The resulting data for the test cases is listed in Table IV.

Table IV. Dataset used to determine the secondary side heat transfer coefficient

Test	p_{Prim} [MPa]	time [s]	T_{wall} [K]	T_{Bulk} [K]	$q\left[\frac{kW}{m^2}\right]$
1	**1,0**	**2100**	**421**	**308**	**117**
2	**3,0**	**1200**	**461**	**323**	**252**
3	**5,0**	**1600**	**459**	**340**	**291**
4	**6,5**	**1000**	**481**	**345**	**397**

Figure 5 shows a comparison of the heat transfer coefficients for the models in Table II with the experimental values from the Noko Test facility for the different pressures examined in the tests. It can be seen that all correlations overestimate the heat transfer coefficient, sometimes very significantly. The value calculated using the Labuntsov [37] correlation comes closest to the experimental values. Nevertheless, even these values are not sufficiently accurate. Therefore, with the help of a regression and the data from experiments 1, 2, and 3 from Table III an improved correlation was developed based on the Labuntsov [37] correlation. The main parameters influencing the heat transfer were considered. These are the Prandl number Pr, the thermal conductivity of the fluid λ, the density of the vapor ρ_{st}, the evaporation enthalpy r, the kinematic Viscosity ν, and the temperature difference between the outer side wall of the heat exchanger tube and the bulk of the fluid ΔT.

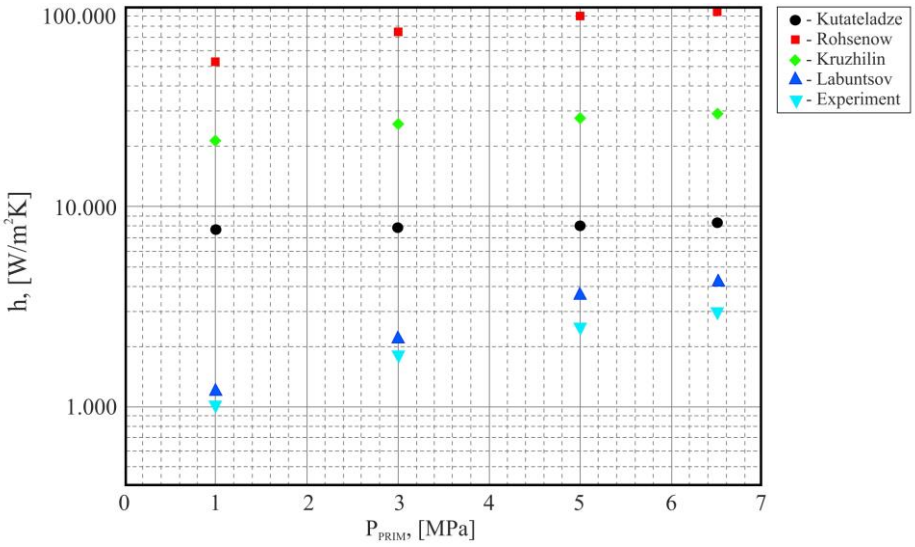

Figure 5. Comparison of the calculated and experimental SS heat transfer coefficient

With this the following form for the Nusselt correlation was selected:

$$Nu = C \cdot Pr^{\alpha} \cdot G^{\beta}; \qquad \text{with } G = \frac{\lambda \cdot \Delta T}{r \cdot \rho_{st} \cdot \nu} \tag{1}$$

The fit-parameter C, α und β were determined by fitting equation (1) with the experimental data – tests 1,2 and 3 listed in Table III. This results in the following values: $C = 1.19005$; $\alpha = 1.3055$; $\beta = 0.879$.

A more detailed description of the regression is given in [33]. With this new correlation and parameters, the heat transfer coefficient for Test 4 (see Table III) at 6.5 MPa was determined. The values are given in Table V and compared with the values resulting from the Labuntsov [37] correlation, the experimental data, and the heat transfer coefficient deduced for the CFD calculation [33]. One can see that again the error for the new correlation is reduced by a factor of 2 compared to the application of the Labuntsov [37] correlation. This represents a much better value and allows us to predict the overall heat transfer with much higher accuracy.

Table V. Comparison of the heat transfer coefficient determined by the new model, the Labuntsov [37] model, the experimental values, and the value derived for CFD calculations.

Test	Labuntsov [37]	New Correlation	Experiment [33]	CFD [33]
4 (6.5 MPa)	**4178** $\frac{W}{m^2 \cdot K}$	**2087** $\frac{W}{m^2 \cdot K}$	**2917** $\frac{W}{m^2 \cdot K}$	**3913** $\frac{W}{m^2 \cdot K}$

4. CONCLUSIONS

Previous assessments of the performance of passive safety systems identified a significant discrepancy between the calculated heat transfer and the measured one. The major reason for that is the inaccurate prediction of the heat transfer coefficient used in such calculations. This paper presents two new models to evaluate the primary and secondary side heat transfer for the Emergency Condenser of the KERENA reactor design. A significant improvement in the prediction of the heat transfer coefficient could be achieved. In the next step, such models will be used to perform the calculation of the heat transfer of the Emergency Condenser performance using the fluid dynamics code ATHELT to show the improved heat transfer prediction. These calculation data will be compared

to published measurement data of the Emergency Condenser performance determined at the INKA test facility [40].

NOMENCLATURE

Roman letters

A	Area [m^2]	L	Characteristic Lengrh [m]
a	Thermal Diffusivity [m^2/s]	m	Mass [kg]
C	Constant	$\dot{m}$	Mass Flow [kg/s]
c_p	Specific heat at constant pressure [J/(kg K)]	Nu	Nusselt Number
D	Diameter [m]	Pr	Prandtl Number
Dh	Hydraulic Diameter[m]	p	Pressure [Pa]
E	Energy Flow [W]	$\dot{q}$	Heat Flux [kW/m^2]
FR	Froude Number	Re	Reynolds Number
f	Pre Factor	Ra	Rayleigh Number
G	Mass Flux [$kg/(m^2\ s)$]	r	Radius [m]
Ga	Galilei Number	S	Momentum Source [N/m^3]
Gr	Grashof Number	s	Length coordinate [m]
g	Gravitational Acceleration [9.81 m/s^2]	T	Temperature [K]
H	Specific Enthalpy [kJ/jg]	t	Time [s]
h	Heat Trasnfer Coefficient [$W/(m^2\ K)$]	u	Velocity [m/s]
Δi_{lv}	Latent Heat [kJ/jg]	X	Martinelli number
Ja	Jakob Number	x	Steam Quality
j_g	Dimensionless gas velocity		

	Subscripts		**Greek**
ann	Annular	Γ	Interphase volumetric mass exc hange [$kg/(m^3s)$]
F	Fluid	α	Gas volume fraction
G	Gas	ε	Void fraction
i	Interface	ε_{mod}	Modified void fraction
l	Liquid	θ	Stratified angle [°]
lam	Laminar	λ	Thermal conductivity [W/(mK)]
m	Mixture	μ	Dynamic viscosity [kg/(ms)]
mean	Average	ϱ	Density [kg/m^3]
sat	Saturation Conditions	σ	Surface tension [N/m]
sec	Secondary Side	τ	Shear stress [N/m^2]
strat	Stratified	δ	Film thickness [m]
trans	Transient		
turb	Turbulent		
v	Vapor		
w	Wall		

REFERENCES

1. INTERNATIONAL ATOMIC ENERGY AGENCY, Passive Safety Systems and Natural Circulation in Water Cooled Nuclear Power Plants, IAEA-TECDOC-1624, Vienna (2009).
2. INTERNATIONAL ATOMIC ENERGY AGENCY, Natural circulation in water cooled nuclear power plants, IAEA-TECDOC-1474, Vienna (2005).
3. P.E. Juhn, J. Kupitz, J. Cleveland, B. Cho, R.B. Lyon, IAEA activities on passive safety systems and overview of international development, Nuclear Engineering and Design 201 (2000) 41–59

4. Z.V. Stosic, W. Brettschuh, U. Stoll, Boiling water reactor with innovative safety concept: The Generation III+ SWR-1000, Nuclear Engineering and Design 238 (2008) 1863–1901
5. T. Mull, T. Wagner, G. Bonfigli, S. Bucholz, F. Schäfer, E. Schleicher, C. Schuster, M. Sporn, Safety cases for design-basis accidents in LWRs featuring passive systems, Nuclear Engineering and Design 327 (2021) 110996
6. Durga Prasad, Gonella V. ; Pandey, Manmohan ; Kalra, Manjeet S.: Review of research on flow instabilities in natural circulation boiling systems. In: Progress in Nuclear Energy 49 (2007), Nr. 6, S. 429–451
7. Hou, Xiaofan ; Sun, Zhongning ; Su, Jiqiang ; Fan, Guangming: An investigation on flashing instability induced water hammer in an open natural circulation system. In: Progress in Nuclear Energy 93 (2016), S. 418–430
8. A. Moonesi Shabestary, F. Viereckl, Y. Zhang, R. Manthey, D. Lucas, C. Schuster, S. Leyer, A. Hurtado, U. Hampel, Modelling of passive heat removal systems: a review with reference to the Framatome BWR reactor KERENA: Part I, Energies, 13 (35) (2020)
9. Manthey, R.; Viereckl, F.; Shabestary, A.M.; Zhang, Y.; Ding, W.; Lucas, D.; Schuster, C.; Leyer, S.; Hurtado, A.; Hampel, U., Modelling of Passive Heat Removal Systems: A Review with Reference to the Framatome BWR Reactor KERENA: Part II. Energies 2020, 13, 109
10. T. Fukano. "THERMOPEDIA, Thermodynamics, Heat and Mass Transfer, and Fluids Engineering," 18 December, 2019.
11. M. M. Shah, “Heat transfer during film condensation in tubes and annuli: the review of the literature,” ASHARE trans, vol. 87, pp. 1086–1105, 1981
12. A. S. Dalkilic, and S. Wongwises, “Intensive literature review of condensation inside smooth and enhanced tubes,” International Journal of Heat and Mass Transfer, vol. 52, no. 15-16, pp. 3409-3426, 2009.
13. T. Geißler, M. Beyer, U. Hampel, H. Prasser, S. Leyer, and M. Walther, “Experimental and numerical investigation of flow structure and heat transfer during high pressure condensation in a declined pipe at COSMEA facility,” in NURETH 16th, pp. 8548–8561, 2015D.E. Author(s), “Article Title,” *Proceedings of Meeting in Italic*, Location, Dates of Meeting, Vol. 31, pp. 134-156 (2012).
14. J. C. Chato, “Laminar Condensation inside Horizontal and Inclined Tubes ”, Massachusetts Institute of Technology, Cambridge, MA, USA.
15. W. Nusselt, “Die Oberflachenkondensation des Wasserdapfes,” Zeitschrift des Vereines Deutscher Ingenieure, vol. 60 pp. 541–575, 1916.
16. G. Lerchel, H. Austregesilo, P. Schöffel, D. von der Cron, and F. Weyermann, “ATHLET: User's Manual,” GRS-P-1 / Vol. 1 Rev. 7, Gesellschaft für Anlagen- und Reaktorsicherheit (GRS) GmbH, (Mar. 2016).
17. "ATHLET Mod 3.1 A: models and methods," GRS, ed., 2016.
18. P. G. Kosky, and F. W. Staub, “Local condensing heat transfer coefficients in the annular flow regime,” J. Heat Transf., vol. 17, pp. 1037–1043, 1971.
19. R. Szijarto, “Condensation of Steam in Horizontal Pipes: Model Development and Validation,” ETH Zurich, Zurich, Switzerland, 2015.
20. M. K. Dobson, and J. C. Chato, “Condensation in smooth horizontal tubes,” J. Heat Transf., vol. 120, pp. 193–213, 1998.
21. A. Cavallini, G. Censi, D. D. Col, L. Doretti, G. Longo, and L. Rossetto, “Condensation of Halogenated Refrigerants Inside Smooth Tubes,” HVAC&R Research, vol. 8, no. 4, pp. 429-451, 2002.
22. A. Cavallini, D. D. Col, L. Doretti, M. Matkovic, L. Rossetto, C. Zilio, and G. Censi, “Condensation in Horizontal Smooth Tubes: A New Heat Transfer Model for Heat Exchanger Design,” Heat

Transfer Engineering, vol. 27, no. 8, pp. 31-38, 2006.
23. M. M. Shah, “An Improved and Extended General Correlation for Heat Transfer During Condensation in Plain Tubes,” HVAC&R Research, vol. 15, no. 5, pp. 889-913, 2009.
24. T.-H. Ahn, B.-J. Yun, J.-J. Jeong, K.-H. Kang, Y.-S. Park, J. Cheon, and D.-W. Jerng, “Development of a new condensation model for the nearly-horizontal heat exchanger tube under the steam flowing conditions,” International Journal of Heat and Mass Transfer, vol. 79, pp. 876-884, 2014.
25. Y. Zhang, INVESTIGATION OF CONDENSATION PROCESS INSIDE INCLINED TUBE, Dissertation Manuscript, University of Luxembourg, 2020
26. T. Tandon, H. Varma, and C. Gupta, “A new flow regime map for condensation inside horizontal tubes.,” J. Heat Transf., vol. 104, pp. 763–768, 1982.
27. B.-U. Bae, S. Kim, Y.-S. Park, and K.-H. Kang, “Integral effect test and code analysis on the cooling performance of the PAFS (passive auxiliary feedwater system) during an FLB (feedwater line break) accident,” Nuclear Engineering and Design, vol. 275, pp. 249-263, 2014.
28. S. Kim, B.U. Bae, Y.S. Park, B.D. Kim, and K.H. Kang, Integral effect test on operational performance of the PAFS (passive auxiliary feedwater system) for a SLB (steam line break) accident, Korea Atomic Energy Research Institute, Daejeon, Republic of Korea, 2012.
29. S. Kim, B.-U. Bae, Y.-J. Cho, Y.-S. Park, K.-H. Kang, and B.-J. Yun, “An experimental study on the validation of cooling capability for the Passive Auxiliary Feedwater System (PAFS) condensation heat exchanger,” Nuclear Engineering and Design, vol. 260, pp. 54-63, 2013
30. J. Hart, P.J. Hamersma, and J.M.H. Fortuin, “Correlations predicting frictional pressure drop and liquid holdup during horizontal gas–liquid pipe flow with a small liquid holdup,” Int. J. Multiphase Flow, vol. 15, pp. 947–964, 1989.
31. F.W.Dittus, and L. M. K. Boelter, “Heat Transfer in Automobile Radiators of the Tubular Type,” International Communications in Heat and Mass Transfer, vol. 12, no. 1, pp. 3-22, 1985.
32. A. Moonesi Shabestary, A. Bieberle, D. von der Cron, W. Ding, E. Krepper, D. Lucas, and U. Hampel, “Flow morphology and heat transfer analysis for high-pressure steam condensation in an inclined tube part II: Numerical investigations,” Nuclear Engineering and Design, vol. 362, 2020.
33. T. Adili, THERMAL HYDRAULIC ANALYSIS FOR ENHANCING PASSIVE HEAT REMOVAL SYSTEMS, Dissertation Manuscript, University of Luxembourg, 2024
34. S. S. Kutateladze, V. M. Borishanskii, and A. d JB, “A concise encyclopedia of heat transfer,” 2021.
35. W. M. Rohsenow, “A method of correlating heat-transfer data for surface boiling of liquids,” Transactions of the American Society of Mechanical Engineers, vol. 74, no. 6, pp. 969-975, 1952.
36. G. Kruzhilin, “Free-convection transfer of heat from a horizontal plate and boiling liquid,” Doklady AN SSSR (Reports of the USSR Academy of Sciences), vol. 58, no. 8, pp. 1657-1660, 1947.
37. D. Labuntsov, “Heat transfer problems with nucleate boiling of liquids,” Therm. Eng.(USSR)(Engl. Transl.), v. 19, no. 9, pp. 21-28, 1973.
38. A. Schaffrath, and H.-M. Prasser, “Theoretical support to the NOKO experiments,” 1998.
39. H. A. T. Hollands, C. Bals, S. Buchholz, S. Ceuca, H. Hristov, A. Langenfeld, P. Pandazis, S. Palazzo, J. Preuß, L. Tiborcz, S. Weber, Validierung von Rechenprogrammen zur Simulation des Reaktorkühlkreislaufs unter Störund Unfallbedingungen, GRS, 2016.
40. R. Bryk, H. Schmidt, T. Mull, T. Wagner, I. Ganzmann, and O. Herbst, “Modeling of KERENA emergency condenser,” Archives of Thermodynamics, vol. 38, no. 4, pp. 29–-51, 2017.